ACSNANO

www.acsnano.org

ARTICLE

Nanoparticle-Induced Disorder at Complex Liquid–Liquid Interfaces: Effects of Curvature and Compositional Synergy on Functional Surfaces

Colin M. Basham,[▽] Uvinduni I. Premadasa,[▽] Ying-Zhong Ma, Francesco Stellacci, Benjamin Doughty,* and Stephen A. Sarles*

Cite This: *ACS Nano* 2021, 15, 14285–14294

Read Online

ACCESS | Metrics & More | Article Recommendations | Supporting Information

ABSTRACT: The self-assembly of surfactant monolayers at interfaces plays a sweeping role in tasks ranging from household cleaning to the regulation of the respiratory system. The synergy between different nanoscale species at an interface can yield assemblies with exceptional properties, which enhance or modulate their function. However, understanding the mechanisms underlying coassembly, as well as the effects of intermolecular interactions at an interface, remains an emerging and challenging field of study. Herein, we study the interactions of gold nanoparticles striped with hydrophobic and hydrophilic ligands with phospholipids at a liquid–liquid interface and the resulting surface-bound complexes. We show that these nanoparticles, which are themselves minimally surface active, have a direct concentration-dependent effect on the rapid reduction of tension for assembling phospholipids at the interface, implying molecular coassembly. Through the use of sum frequency generation vibrational spectroscopy, we reveal that nanoparticles impart structural disorder to the lipid molecular layers, which is related to the increased volumes that amphiphiles can sample at the curved surface of a particle. The results strongly suggest that hydrophobic and electrostatic attractions imparted by nanoparticle functionalization drive lipid–nanoparticle complex assembly at the interface, which synergistically aids lipid adsorption even when lipids and nanoparticles approach the interface from opposite phases. The use of tensiometric and spectroscopic analyses reveals a physical picture of the system at the nanoscale, allowing for a quantitative analysis of the intermolecular behavior that can be extended to other systems.

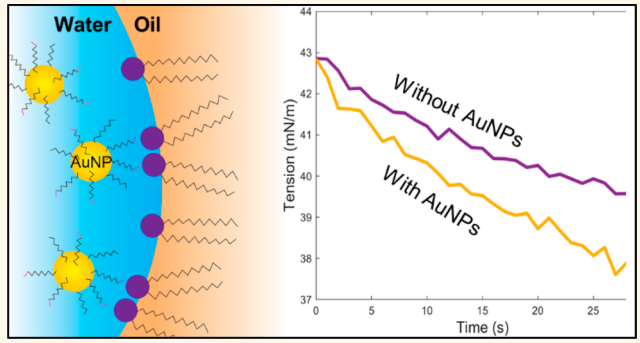

KEYWORDS: *phospholipid monolayer, interfacial tension, amphiphilic gold nanoparticles, sum frequency generation spectroscopy, multiple species adsorption, liquid–liquid interface*

The collective interactions of molecular and nanoscale constituents at a fluid interface represent a key set of complicated, yet technologically important, handles that may be used to impart a function into otherwise benign species. For instance, the coassembly of nanoparticles and surfactants is of commercial importance for stabilizing emulsions[1] and controlling the morphologies of soft materials,[2] while functionalized nanoparticles offer vast potential in targeting membrane-bound cancer receptors.[3,4] The tunability of a nanoparticle's size,[5] shape,[6] and composition[7,8] affords control for engineering molecular interactions while simultaneously presenting challenges in their separation from complex chemical mixtures in waste remediation or chemical reactions.[9,10] The breadth of these complex behaviors is often realized at an *additional* interface that imparts functionality to the molecular species via the macroscopic chemical and physical asymmetry. As such, knowledge of how interfacial variables affect function is the key to understanding nanoparticle-mediated assembly, reactivity, and transport.

Received: March 29, 2021
Published: September 13, 2021

https://doi.org/10.1021/acsnano.1c02663
ACS Nano 2021, 15, 14285–14294

In a biological setting, the influence of nanoparticles on passive and active processes at cellular interfaces is of particular importance. Recently, Stellacci et al. demonstrated that <10 nm spherical gold nanoparticles (AuNPs) with localized striations of hydrophilic and hydrophobic ligands are able to passively translocate the cell membrane, thereby entering the cytosol and carrying payloads via a nonendocytic and nondestructive pathway.[11] This finding, along with other more recent work,[12] suggests that nanoparticle size and amphiphilicity—controlled via surface decoration by ligands—are key to tuning their bioactivities. Molecular dynamics simulations on striated amphiphilic nanoparticles suggest that electrostatic and hydrophobic interactions[13,14] between the striped particles and membrane lipids play a pivotal role in the penetration and translocation of the bilayer.

However, far fewer experimental studies[13,15] aimed at revealing and quantifying nanoscale interactions between amphiphilic nanoparticles and model membranes (*e.g.*, lipid monolayers and bilayers) have been performed, and evidence for characterizing passive membrane translocation by striped amphiphilic particles[11,16] remains elusive. As such, an investigation of nanoscale interactions between amphiphilic nanoparticles and phospholipids is needed to explain their ability to enter cells and to validate the use of model membranes for accurately depicting nanoparticle functionality. Moreover, the same mechanisms of cellular translocation are parallel to understanding nanoparticle−surfactant behaviors in liquid extractions, separations, and synthetic chemistry. We anticipate the results of such investigation will support a broader understanding of amphiphile−nanoparticle interactions at buried liquid−liquid (L/L) interfaces, which remain poorly understood due to technical challenges and limited accessibility.[17−22]

Therefore, seeking to address these knowledge gaps, we report on collective self-assembly behaviors exhibited by ligand-coated nanoparticles and phospholipids at an oil−aqueous interface, which more closely mimics the fluidity and hydrophobicity of a lipid bilayer through *n*-alkane oils than an air−water system.[23] Specifically, we show via pendant drop tensiometry that the aforementioned striped amphiphilic AuNPs (2−3 nm in core diameter), which display little surface activity on their own, enhance the dynamic adsorption of lipids to form a densely packed lipid monolayer at the oil−aqueous interface. This phenomenon is dependent on the concentration of AuNPs as well as the degree of hydrophobic ligand functionalization on the surface of the nanoparticles. We explore these interactions using both 1,2-diphytanoyl-*sn*-glycero-3-phosphocholine (DPhPC) and 1,2-dioleoyl-*sn*-glycero-3-phosphocholine (DOPC) lipids, which are frequently chosen for the formation of durable[24] and biologically relevant[15] model membranes, respectively, at room temperature. Fitting the initial diffusion-limited adsorption data quantitatively reveals the collective influence of AuNPs and lipids on the rate of assembly for the lipid monolayer. Interestingly, this effect is present regardless of whether lipids and nanoparticles inhabit the same or opposing liquid phases, which suggests that a synergy occurs between the two species at the interface. Complementary measurements of the oil−aqueous interface using vibrational sum frequency generation (SFG) spectroscopy further reveal how AuNPs affect the ordering of lipid acyl chains, suggesting that the two species cooperate to form interfacially active complexes that mediate lipid adsorption. This study provides insight into how the presence of molecular surfactants and other nanoscale species can assist in the assembly of structural motifs and chemical compositions observed at equilibrated interfaces.

RESULTS AND DISCUSSION

For pendant drop measurements of the interfacial tension, we employed two types of AuNPs either coated by hydrophilic 11-mercapto-1-undecanesulfonate (MUS) ligands only, which contained negative charges on the terminal sulfonate groups, or decorated with both hydrophilic MUS and hydrophobic 1-octanethiol (OT) ligands at a molar ratio of 85:15 MUS:OT; hereafter, these variants are designated as 0%OT or 15%OT AuNPs, respectively. The ligands are covalently attached to the AuNPs via thiol bonds, and their structures are shown in Figure S1 along with those of the lipids. Both AuNP types are readily soluble in water; however, it was found that AuNPs with ≥30% hydrophobic OT ligands required ethanol for dissolution. Since alcohols can modify the wettability of particles and thus their behavior at an oil−aqueous interface,[25] these AuNPs were excluded from interfacial tension measurements.

Figure 1a shows the dynamic reduction in the interfacial tension at the oil−aqueous interface versus time when 1 mM

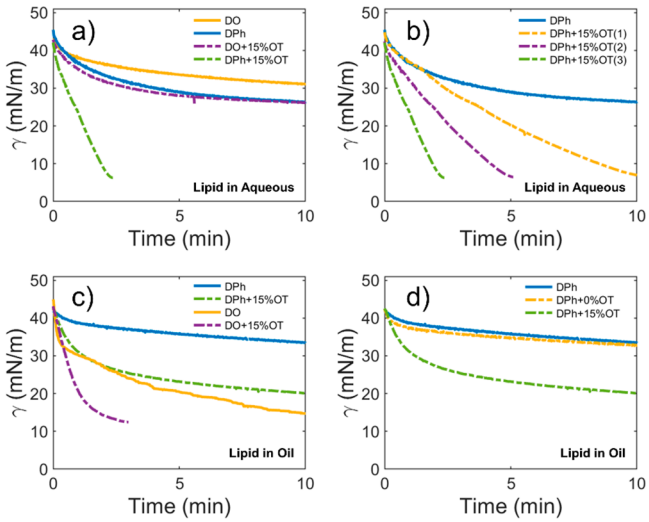

Figure 1. Nanoparticles influence phospholipid adsorption, as evidenced through rapid decreases in the interfacial tension. In these plots, lipid concentrations are 1 mM, and all AuNP concentrations are 0.5 mg/mL unless otherwise stated. (a) When lipids are present in the aqueous phase, the inclusion of 15%OT AuNPs enhances the adsorption of both DOPC and DPhPC. (b) Increasing the concentration of 15%OT AuNPs from (1) 0.005 to (2) 0.05 to (3) 0.5 mg/mL increases adsorption rates of DPhPC in the aqueous phase. (c) When lipids are instead present in the oil phase, 15%OT AuNPs in the aqueous phase still enhance adsorption rates of both DOPC and DPhPC. (d) The hydrophilic 0%OT AuNPs enhance the adsorption rate of DPhPC in the oil phase but not as drastically as the 15%OT particles do at the same concentration.

DOPC or DPhPC liposomes are provided in the aqueous phase. This lipid concentration is well above the critical micelle concentration, which was found to be between 1 and 10 μM for both lipids.[26] These measurements reveal that the interfacial tension decreases slightly faster when DPhPC lipids are present compared to when DOPC lipids are present. This

https://doi.org/10.1021/acsnano.1c02663
ACS Nano 2021, 15, 14285−14294

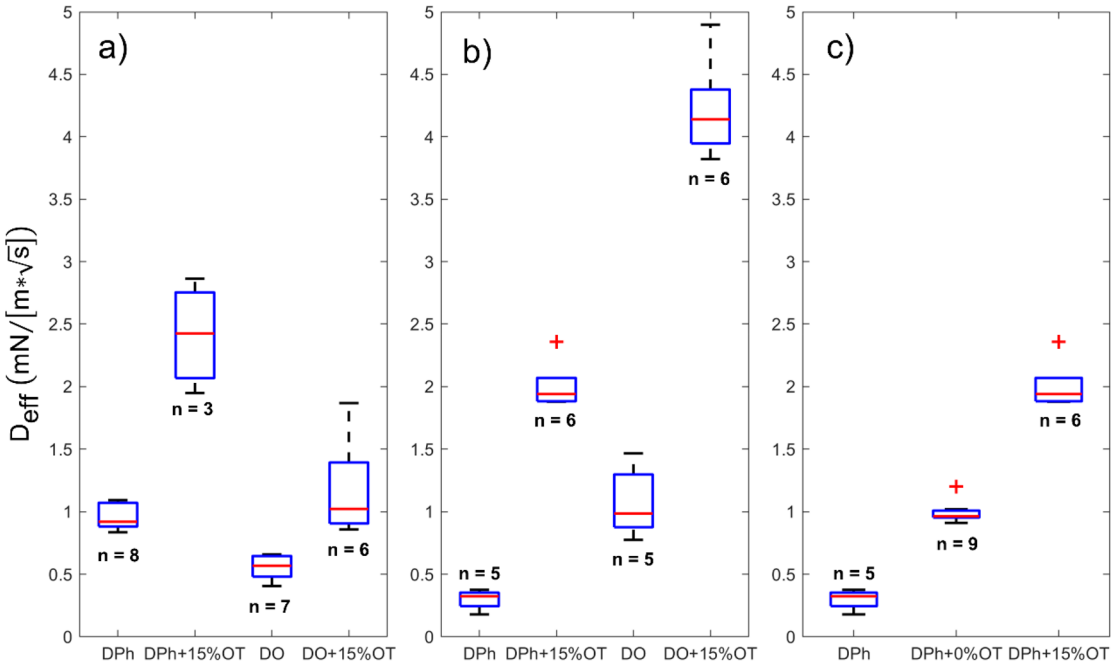

Figure 2. Adsorption rates, D_{eff}, in the diffusion-limited adsorption regime. The red lines designate population medians, while the "+" symbols show outliers. The number of trials per condition is indicated outside each box. The whiskers extend to approximately $\pm 2.7\sigma$, i.e., the standard deviation, and encompass 99.3% of all data points in the normal distribution. All AuNPs are at a 0.5 mg/mL concentration, and all lipids are at a 1 mM concentration. (a) Comparison of D_{eff} for DPhPC and DOPC in buffer with and without 15%OT AuNPs in the aqueous phase. (b) Comparison of D_{eff} for DPhPC and DOPC in oil with and without 15%OT AuNPs in the aqueous phase. (c) Comparison of D_{eff} for DPhPC in oil with either 0%OT AuNPs or 15%OT AuNPs in the aqueous phase.

is likely due to the longer acyl tail lengths in DOPC, which decrease its solubility in water and therefore the molecular release rates from liposomes.[27] When 0.5 mg/mL 15%OT AuNPs were added to the aqueous solution in addition to 1 mM lipids, the rates of change of the interfacial tension noticeably increased (Figure 1a) for both DOPC and DPhPC present in the aqueous phase. The extent of this increase was strongly dependent on the concentration of nanoparticles (Figures 1b and S2) in the aqueous phase, confirming that the nanoparticles directly impact the reduction in the interfacial tension in the presence of lipids. Without lipids, however, the interfacial tension measured in the presence of AuNPs matches that of the neat hexadecane−aqueous buffer interface regardless of the ratio of hydrophilic to hydrophobic functionalized ligands (Figure S2). The buffer for all experiments was 1× PBS (see Methods). Therefore, while AuNPs do not act as a surfactant on their own, these data reveal that combining 15%OT AuNPs and lipids increases their mutual interfacial activity at the oil−aqueous interface.

With the placement of both nanoparticles and lipids in the aqueous phase, it was not possible to discern *how* AuNPs affect adsorption. Previous studies have shown that silica nanoparticles and palmitic acid bind to form complexes in the bulk,[28] thereby altering the interfacial tension at the oil−aqueous interface. Furthermore, nanoparticles have been shown to induce hemifusion and aggregation in lipid vesicles.[29,30] Therefore, to determine if the rapid reduction of the interfacial tension was mediated by the formation of nanoparticle−lipid aggregates in the aqueous bulk, separate measurements were performed where phospholipids were instead dissolved in hexadecane to study the adsorption of lipids from the neighboring liquid phase. Figure 1c shows representative traces of the interfacial tension versus time at an oil−aqueous interface constructed from hexadecane that contained 1 mM DOPC or DPhPC lipids. Here, DOPC was found to reduce the interfacial tension slightly faster than DPhPC, which suggests a difference in the energetic favorability for adsorption.[31] Yet, when 0.5 mg/mL 15%OT AuNPs were added to the aqueous phase, we once more observed that the rate of reduction in the interfacial tension was enhanced. Notably, these results show that the nanoparticle-assisted reduction in the interfacial tension did not require nanoparticle−lipid interactions in a shared bulk phase, *i.e.*, any effect of AuNPs on the structure or net charge of liposomes was not the dominant factor for the enhanced adsorption when both were present in aqueous buffer. Instead, the measurements suggest there exist complementary interactions between the two species at the macroscopic oil−aqueous interface.

The impact of nanoparticle hydrophilicity on lipid-mediated reductions in interfacial tension was also studied. In Figure 1d, measurements showed that 15%OT AuNPs present in the aqueous phase resulted in faster interfacial tension reductions compared to either an equal concentration (0.5 mg/mL) of 0% OT AuNPs or no AuNPs with 1 mM DPhPC lipids present in the oil. Thus, the cooperative interfacial activity of lipids plus AuNPs at the interface is strengthened by the presence of hydrophobic ligands on the nanoparticle.

Quantifying the diffusion rates during multiple stages of surfactant adsorption can give insight into when AuNPs affect lipid assembly. In the absence of external influences, such as molecular crowding or interfacial charge accumulation, the limiting rate of surfactant adsorption is diffusion from the bulk to the subsurface, which is directly adjacent to the interface. Transfer from the subsurface to the surface is taken to be spontaneous, allowing this diffusion-limited adsorption to be

https://doi.org/10.1021/acsnano.1c02663
ACS Nano 2021, 15, 14285−14294

modeled with a short-time approximation of the Ward−Tordai equation (see eq 1 in Methods). The Henry isotherm,[32] which relates the surface density of a surfactant to the surface tension, is applicable only at these short times because it does not account for finite adsorption spaces or lateral surface interactions at the interface. We assume that nanoparticles do not behave as surfactants since they display negligible surface activity, as shown in Figure S2 and supported by the SFG data presented below. Therefore, the parameter c_0 in eq 1 represents only the bulk phospholipid concentration, making the effective diffusion coefficient D_{eff} an accurate measurement of lipid short-term adsorption and allowing us to determine when nanoparticles begin to affect the adsorption process. Further, D_{eff} allows for comparisons of the adsorption even when single phospholipids and lipid aggregates are present simultaneously, since the lipid concentration is the same across all experiments. A similar analysis was used for mixed surfactant systems.[33,34]

The effective rate of lipid diffusion-limited adsorption was calculated using eq 1 for all interfacial tension test conditions, as demonstrated in Figure S3, and is compared in Figure 2. From Student's *t*-tests of the D_{eff} data, we determined that the effective adsorption rates are statistically different ($p < 0.05$) for both DPhPC and DOPC in the presence of aqueous 15% OT AuNPs, in both lipid-in-buffer and lipid-in-oil scenarios, when compared to those of respective control cases. The 0% OT AuNPs also caused a statistically significant increase in the D_{eff} of the DPhPC adsorption from the oil phase even though it was less than the rate increase for DPhPC when 15%OT AuNPs were present (Figure 2c). From these comparisons, we can conclude that there is an immediate enhancement of lipid adsorption to a dilute interface when nanoparticles are present in the aqueous phase in addition to a dependence of the AuNP ligand functionalization on the measured rate. This suggests that while the AuNPs do not strongly impact the interfacial tension on their own, they are likely present *near* the surface such that they can couple with lipids from the bulk phase to form complexes that are strongly surface active to a degree that is more than the sum of the parts. In other words, there is a synergy between the AuNPs and the lipids, and the oil−aqueous interface allows for chemical or structural motifs to emerge that alter the interfacial tension and structural composition.

The minimum interfacial tension is often an indicator of an equilibrated system and can give insight into the molecular packing and area per molecule of surfactants at the interface. To gauge whether 0%OT and 15%OT AuNPs remained present at the interface near equilibrium, we evaluated the minimum interfacial tension of 1 mM DOPC in the oil phase with AuNPs either absent or present (0.5 mg/mL) in the aqueous phase. The minimum tension for 1 mM DOPC at a neat oil−aqueous interface, with a single standard deviation, was 0.69 ± 0.12 mN/m ($n = 7$). For a DOPC and 0%OT interface the minimum tension was 0.56 ± 0.26 mN/m ($n = 3$), while for a DOPC and 15%OT interface the minimum tension was 0.57 ± 0.05 mN/m ($n = 5$). Student's *t*-tests showed that the only statistical difference ($p < 0.05$) for these populations was between DOPC-only lipid monolayers and DOPC+15%OT AuNPs, implying that 15%OT AuNPs affect the interface by decreasing interfacial tension at equilibrium while 0%OT AuNPs do not. It should be noted, however, that these values are at the limit of sensitivity for the pendant drop tensiometer. Since the tension of the neat oil−aqueous interface, γ_0, is approximately 42 mN/m (Figure S2), these equilibrium tensions correspond to a surface pressure of $\Pi = \gamma_0 - \gamma \approx 41$ mN/m, which is in close agreement with the value for a fully packed phosphocholine (PC) monolayer.[31] To further evaluate the reversibility of AuNP−lipid complex adsorption, and to determine the ability of these complexes to jam at the interface as has been reported by others,[35] we let a pendant droplet interface comprised of 15%OT AuNPs and DOPC approach equilibrium and then retracted the volume to laterally compress the saturated monolayer (Figure S4). For these conditions, "wrinkling" of the monolayer was not observed, implying the AuNP−lipid complexes are not fully irreversible and cannot jam the interface into nonequilibrium shapes in contrast to several other nanoparticle−surfactant systems.[36,37]

To provide chemical insight into these interfaces and complement the macroscopic nature of pendant drop tensiometry, we performed SFG measurements at the buried liquid−liquid interface. Here, we used aqueous AuNPs functionalized with hydrophilic and hydrophobic ligands in 100:0, 85:15, and 70:30 ratios (0%OT, 15%OT, and 30%OT, respectively). While the 30%OT AuNPs required ethanol for dissolution, time-resolved SFG spectra showed that ethanol was quickly replaced by lipids at the interface (see Figure S5). The SFG spectra shown in Figure 3 were obtained at an

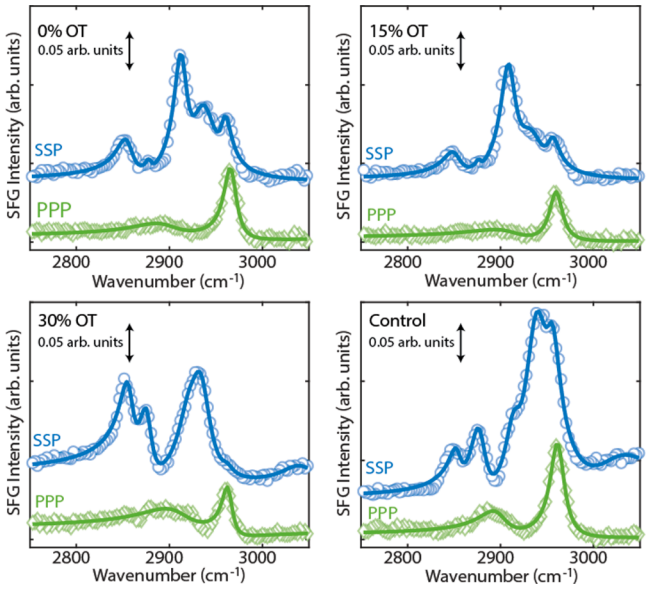

Figure 3. SFG spectra of the buried L/L interface in the presence of AuNPs in the aqueous phase with variable OT coverages, as indicated by the labels in the top left corner of the plots. The control spectra were taken in the absence of AuNPs and thus probe lipids at the oil−aqueous interface. Spectra are offset for clarity. Points are measured data, and the solid lines are fits.

equilibrated DOPC lipid interfacial layer in both the presence and absence of the three types of AuNPs. The two phases were in contact for a *minimum* of 150 min prior to these measurements, which is longer than the time needed to reach the minimum interfacial tensions. The peaks observed in the SSP spectrum correspond predominantly to symmetric stretching modes of the $-CH_2$ and $-CH_3$ groups on the lipids and potentially to the capping groups of the ligands grafted to the AuNPs.[18] Notably, peaks near 2850 cm^{-1} correspond to the symmetric stretch of the $-CH_2$ groups in the alkyl chains,

https://doi.org/10.1021/acsnano.1c02663
ACS Nano 2021, 15, 14285−14294

whereas the peak near 2875 cm^{-1} corresponds to the $-CH_3$ symmetric stretch. Peaks at higher frequencies (*i.e.*, those near 2900−2950 cm^{-1}) correspond to Fermi resonances (FRs) with weak contributions from out-of-phase asymmetric stretches.[38] The splitting of these higher frequency peaks into resolvable resonances *qualitatively* reports on the different intermolecular interactions and couplings that manifest at the different interfaces;[39] however, due to the spectral complexity and unresolved contributions from the aforementioned asymmetric stretches, we do not quantify these interactions. The PPP spectra show a sharp peak near 2965 cm^{-1} that corresponds to the asymmetric stretch of the $-CH_3$ group and a broad feature near 2900 cm^{-1} that corresponds to the $-CH_2$ asymmetric stretch. The broad feature extending from beyond 3000 cm^{-1} is due to the −OH stretches of interfacial water. We did not observe a broad nonresonant response from the AuNPs at the oil−aqueous interface, as was recently reported for dried AuNP−lipid films.[40] Instead, our observation is consistent with previous reports that show, upon scaling the SFG spectrum with a nonresonant reference spectrum, that nonresonant contributions should manifest as a spectrally flat baseline.[41,42] In the absence of an oil phase, and therefore lipids, we do not see evidence for adsorption of the AuNPs to the air−aqueous interface regardless of the nanoparticle surface functionalization (data in Figure S5), which is in agreement with surface tension measurements at oil−aqueous interfaces (Figure S2). In the presence of both oil and lipid, we find that for all cases that the SFG signals are intense even in the absence of AuNPs. We note that all aqueous solutions contained PBS buffer at equivalent ionic strengths and pH levels to ensure that potential ion pairing and H-bonding interactions were the same between measurements and systems. Since SFG is sensitive to interfacial asymmetry and population, here the measured signals correspond to a convolution of surface coverage and the interfacial packing.

To disentangle these factors, we consider the extracted intensities by fitting the data to eq 2. First, we consider the ratio of the measured $-CH_3$ asymmetric stretch obtained in the PPP polarization combination to the $-CH_3$ symmetric stretch measured from the SSP spectrum. The ratio removes the concentration dependence in the SFG response and can be used to calculate the average $-CH_3$ tilt angles,[38,43] which are plotted in Figure 4a for the different aqueous phase conditions. The extracted peak positions and average orientational angles obtained from SFG measurements agree with those previously reported[17,44,45] and with expectations based on the amphiphilic nature of the lipids and ligands in the system. For a macroscopically flat interface, one would expect to find the acyl tails of the lipids standing more upright such that the average $-CH_3$ tilt angle assumes smaller angles with respect to the normal. This conformation allows for the highest coverage of amphiphiles at the interface. However, at a locally curved interface, such as around an embedded AuNP near the surface, a larger conical volume can be sampled by a given lipid or ligand tail without steric hindrance from a neighbor, as sketched in Figure 5. As such, one would expect larger average orientational angles for the $-CH_3$ groups in the presence of AuNPs. This effect is found in the data plotted in Figure 4a, which shows for the AuNP-free sample (control) the lipid tail ends assume orientational angles closer to the surface normal, whereas the presence of AuNPs results in larger average $-CH_3$ angles that grow as the %OT ligand coverage decreases. This trend implies that the *coating* on the AuNP plays a role in the

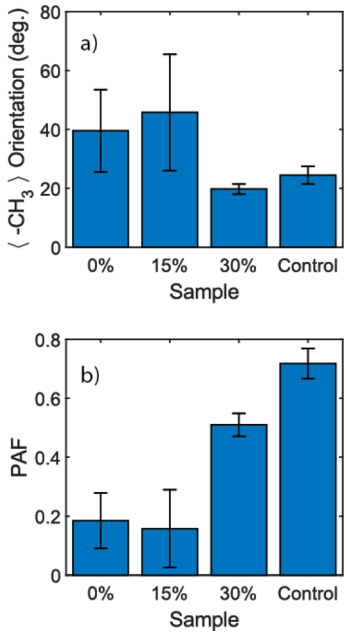

Figure 4. (a) Average methyl orientational angle calculated from the measured SFG intensities at equilibrium. (b) Peak area fraction (PAF), an ordering parameter, for the different sample interfaces studied. Larger values indicate better ordering of the lipid tails.

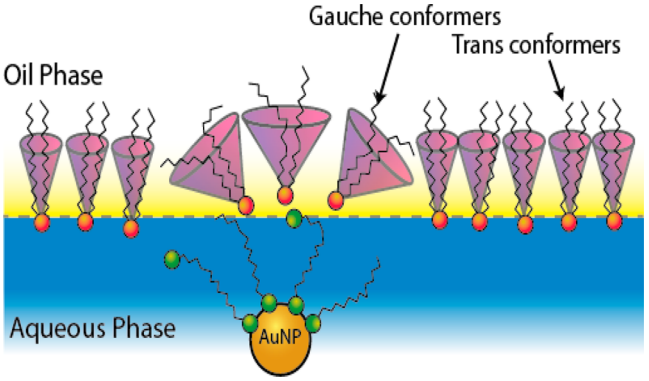

Figure 5. The presence of AuNPs at a macroscopic interface disrupts the nominal orientation of lipids at equilibrium. The purple shaded cones represent volumes that can be sampled by the alkyl tails; the curvature of the AuNP allows for larger volumes to be sampled without an interaction with neighboring ligands or lipids.

structuring of the lipids and does not arise purely from the nanoparticle itself. We note that changing the interfacial index of refraction to 1.38 (the average of the water and hexadecane bulk indices of refraction) changes the average orientational angles by only a few degrees toward the normal, whereas the trend in the orientational angles does not change. We also assume a real interfacial index of refraction due to the off-resonance excitation and emission wavelengths relative to the AuNP core plasmon resonance.

To elaborate on the trends observed in the orientational angles, we consider an ordering parameter known as the peak area fraction (PAF = $A_{CH3}/(A_{CH3} + A_{CH2})$) that qualitatively relates to the number of gauche conformers in the tails. A measured PAF closer to unity represents fewer gauche conformers and a more ordered monolayer, whereas measured

https://doi.org/10.1021/acsnano.1c02663
ACS Nano 2021, 15, 14285−14294

PAFs approaching zero describe a poorly ordered surface with tails sampling large conical volumes. From the data in Figure 4b, we find that the presence of AuNPs lowers the PAF, resulting in an apparent increase in the number of gauche conformers that is characteristic of adsorption to a curved surface.[18,41,46] Specifically, we find that for low %OT particles, the lipids interact with the AuNPs localized near the oil–aqueous interface to form a loose coating of lipids. In contrast, the 30%OT samples present fewer charged hydrophilic ligands to the zwitterionic phosphocholine headgroups at the interface and thus do not interact as strongly, such that the lipids retain a better packed structure with a correspondingly larger PAF. In the absence of AuNPs (control), the PAF of the lipid assembly reaches a maximum, as expected, based on the lack of interfacial curvature presented by nearby nanoparticles. This is in support of the orientational results presented above and is sketched qualitatively in Figure 5. Upon adsorbing onto AuNPs, lipid tails will sample larger conical volumes, compensating for energy changes associated with loss of prevailing noncovalent bonds via entropic effects.

The SFG results presented to this point describe the *equilibrated* interfacial structures but do not describe dynamic structure formation or provide a mechanism by which to rationalize the differences and connect them to interfacial tension measurements. To complement the time-resolved tension data, time-resolved SFG spectra were taken *during* the assembly of the lipids at the L/L interface and are presented in Figure 6. Here we plot SFG spectra collected at evenly spaced time intervals throughout the assembly process, starting immediately after deposition of the lipid or oil phase on the aqueous subphase. The complete data series is provided in the Supporting Information as Figure S6. Notably, the SFG signal in the absence of AuNPs (control) shows near time-invariant signals. This means that (1) the surface is nearly saturated with amphiphilic species within the first few minutes and (2) subtle changes in packing or the sample height are responsible for the changes to the interface over much longer time scales. Moreover, the fact that the time-resolved SFG signal does not decay suggests that the measured dynamics are those of a monolayer assembly (a molecular interface with asymmetry) and are not due to the formation of centrosymmetric assemblies (*e.g.*, micelles or bilayers).[17]

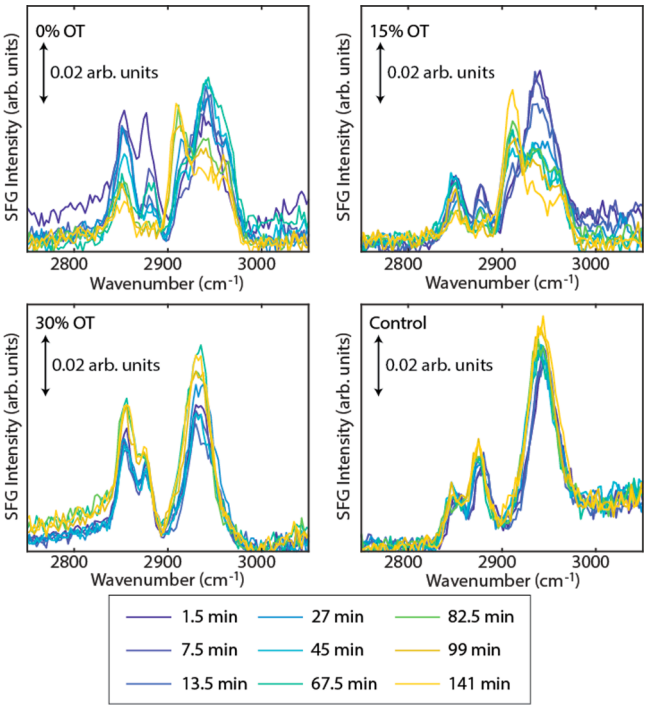

Figure 6. Time-resolved SFG spectra of the buried L/L interface in the presence of AuNPs in the aqueous phase with variable %OT coverages, as indicated in each plot.

In the presence of 30%OT AuNPs, we find that the signal changes only subtly with an overall increase in the SFG response and has qualitatively invariant $-CH_2/-CH_3$ peak ratios. While the 30%OT sample also contained small amounts of ethanol (data shown in Figure S5), the signals observed in Figure 6 are similar to the control results, only showing different relative peak ratios. This indicates that (1) the lipids efficiently displace the ethanol that initially occupies the interfacial monolayer; (2) the interface is perturbed from the presence of AuNPs coadsorbing or binding to lipids, which facilitates the incorporation of modest levels of gauche conformers (see Figure 4b); and (3) the time-resolved symmetry and ordering of the amphiphiles at the interface is lower in the presence of AuNPs than at the neat surface. The increased SFG signals could arise from an increase in the interfacial lipid concentration that interacts with the nanoparticles, which offer larger surface areas versus their footprint at the interface, or enhancements due to plasmonic and scattering effects that would become more pronounced as particles partition to the surface. These results suggest that lipids adsorb to the oil–aqueous interface where they attract nanoparticles from the nearby aqueous phase and subsequently disrupt the interfacial layer. This mechanism is more dramatic in the 0%OT and 15%OT systems, where the $-CH_3$ symmetric stretching peaks (~2875 cm^{-1}) are clearly visible in both systems at early times; however, as the interface assembles, the relative intensity of the $-CH_2$ peak increases and that of the $-CH_3$ peak decreases, which is indicative of lower PAFs and more interfacial disorder or gauche conformers. The peaks found above 2900 cm^{-1} correspond to FRs and asymmetric stretches that show an obvious transition from a single dominant peak to at least three partially resolved peaks. The dominant FR bands found are attributed to the lipids initially adsorbed to the oil–aqueous interface since they were always observed in measurements at early times (and in the control). The splitting of this peak could be due to increased FR contributions from $-CH_2$ groups that would grow with the decreasing interfacial symmetry facilitated by the presence of curved nanoparticle interfaces. This would be seen as a peak close to 2920 cm^{-1}, which is indeed found to increase versus time for the 0%OT and 15%OT samples. Given the nature of FRs and their sensitivity to local chemical environments, this spectral region could potentially be used as a probe for interfacial interactions on an inter- and intramolecular level; however, this lies beyond the scope of this work due to the aforementioned complexities in peak assignment and heavy dependence on accurate theories to quantify these effects.

Considering the time-resolved SFG responses during the lipid assembly and the static measurements at the equilibrium state, we observed that the presence of nanoparticles imparts disorder to the interfacial layer. This effect is more pronounced for 0%OT and 15%OT samples, where we observed clear variations in the ordering during assembly and in the equilibrium state (Figures 3 and 6). The near time-invariant

https://doi.org/10.1021/acsnano.1c02663
ACS Nano 2021, 15, 14285–14294

SFG responses from the control and 30%OT samples show minimal variations in ordering from the initial assembly until the equilibrium state.

In summary, both the hydrophilic and amphiphilic AuNPs studied here were minimally surface active at the oil−aqueous interface; as nanoparticles rely on sufficient hydrophobicity to drive their wettability at the interface,[47,48] this result is not surprising. However, incorporating these functionalized AuNPs into a lipid-containing system in either the same or opposing bulk liquid phase rapidly increased the rate of the interfacial tension reduction during the diffusion-limited phase, implying that the coassembly of nanoparticles and lipids at the interface enhances lipid adsorption. We should mention that since the AuNP core is coated in ligands there is likely no special role that the bare Au surface plays in adsorption. This means that other NPs could conceivably be used in the same manner, provided that a similar degree of NP surface functionalization could be achieved. Since the rate increase was larger with 15% OT AuNPs compared to 0%OT AuNPs, the data suggest that hydrophobic ligands on the surface of a NP increase its ability to interact with the interface, perhaps by providing both hydrophobic and hydrophilic handles for complex formation with amphiphilic lipids. Molecular dynamics (MD) simulations indicate that hydrophobic OT ligands on 3−4 nm nanoparticles display a high conformational flexibility[5,49] and that anisotropic ligand coatings reorient along a water−vapor interface to minimize the free energy.[50] This inherent flexibility allows the OT ligands to align toward the oil phase to reduce contact with water and favors the formation of lipid−nanoparticle complexes that are stabilized by van der Waals attractions with nearby lipid tail groups. The anionic MUS ligands are also tethered by hydrophobic chains, but their bulky terminal sulfonate groups inhibit their conformational flexibility such that they are more likely to remain in the aqueous phase.[5]

While pendant drop tensiometry indicated that sufficiently hydrophobic AuNPs more strongly enhance the rate of lipid self-assembly, SFG measurements confirmed that both 0%OT and 15%OT AuNPs show strong synergistic effects with the phospholipid assembly. The fact that AuNPs were highly negative in 1× PBS buffer, as confirmed by ζ-potential measurements, indicates that electrostatic interactions are key to these responses. In these physiological salt conditions, sodium ions will interact with PC headgroups and screen repulsive negative charges.[51] The beneficial effect of salt on DPhPC adsorption can be seen in Figure S2. We therefore expect the charged MUS ligands to bind electrostatically with the cationic choline headgroups closest to the aqueous bulk during adsorption; indeed, it has been determined through both experimentation[49] and simulation[13,14] that MUS:OT AuNPs show weak electrostatic binding with a DOPC membrane, which heralds membrane translocation. This may explain why the 30%OT AuNPs, which would present less charged ligands and therefore less binding sites toward the lipid headgroups, had the most marginal effect on assembling lipid molecular layers and the resulting PAF of any AuNP functionalization studied. While the adsorption of AuNPs to liposomes in the aqueous phase likely occurs, the rate increase of the surface tension reduction with each molecular species in different bulk phases confirms that bulk interactions are not necessary for interfacial coupling.

The significant differences in D_{eff} during the diffusive adsorption phase show that the AuNPs do not require a partially formed lipid monolayer before assisting lipid adsorption to the interface; rather, it is likely that they present a handle for immediate phospholipid coupling. Thus, the drastic change in dynamic interfacial tension results from a balance of (1) the availability of particles near the interface and (2) favorable electrostatic and hydrophobic interactions between AuNPs and lipids. While D_{eff} reflects differences in dynamics during the initial adsorption process, time-resolved SFG measurements show that AuNPs continuously alter the interfacial morphology as the tension continues to decrease. Once the interface becomes sufficiently populated, the assembling surfactant monolayer transitions from diffusion-limited to kinetically limited adsorption, as seen by the short duration of the linear diffusion regime compared to the longer tensiometry plot (Figure S3). Accordingly, time-resolved SFG spectra qualitatively show that the number of gauche conformers at the surface increases over time despite this type of molecular disorder likely being balanced by electric condensation and van der Waals forces. Though these later rates of interfacial tension reduction were not quantified in this study, bound lipid−AuNP complexes are also less likely to dissociate from the interface, resulting in further tension reduction similar to other mixed surfactant systems.[1,36] SFG measurements show that these complexes are present at equilibrium even though the minimum tension is not greatly affected.

CONCLUSIONS

The results of this work showcase a synergy that is possible between surfactants and ligand-decorated nanoparticles when both are present at an oil−aqueous interface; surface-inactive nanoparticles not only accelerated lipid adsorption but also affected lipid morphology in the monolayers due to the formation of lipid−nanoparticle complexes exhibiting surface activities greater than the sum of their parts. Thus, this work suggests that immiscible liquid−liquid interfaces can be strategically used to characterize and control such interactions between other nanoscale constituents, offering broad potential in both commercial and biological applications. Further, these interfaces are common platforms for the synthesis of artificial cell membranes, such that understanding nanoparticle behavior can be considered a foundational step in understanding membrane translocation. Through the pairing of interfacial tension and spectroscopic methods to evaluate a mixed species system comprised of gold nanoparticles and phospholipids at liquid−liquid interfaces, our results emphasize the importance of hydrophobic and electrostatic considerations in nanoparticle synthesis for molecular targeting and nascent surface stabilization even when the nanoparticles themselves are largely surface-inactive. Moreover, they showcase the value in combining these experimental methods to reveal mechanisms and interfacial morphologies not immediately apparent in either individual technique.

METHODS

Materials. Gold nanoparticles with core diameters of 2−3 nm, which were coated with either MUS ligands or a mixture of MUS and OT ligands, were prepared by the Stellacci group as described elsewhere.[11] DPhPC and DOPC were purchased in chloroform from Avanti Polar Lipids. 10× PBS was purchased from Invitrogen, diluted to a 1× concentration (137 mM NaCl, 2.7 mM KCl, 8 mM Na_2HPO_4, and 2 mM KH_2PO_4) with Millipore Sigma Direct-Q deionized water (conductivity of 18.2 MΩ/cm), and pH adjusted

https://doi.org/10.1021/acsnano.1c02663
ACS Nano 2021, 15, 14285−14294

with small amounts of hydrochloric acid to a physiological pH of 7.3. *n*-Hexadecane (Acros) was purchased at 99% purity and filtered with disposable 0.2 μm poly(ether sulfone) membranes (Whatman) prior to use.

Sample Preparation. Nanoparticles were hydrated from a dry state with 1× PBS. The colloidal suspensions were sonicated in a bath for 15 min, then extruded with a Whatman 30 nm polycarbonate membrane using an Avanti Mini Extruder. Samples were stored at 4 °C prior to use. Phospholipids in chloroform were evaporated prior to use with a house vacuum system for 3 h, and the resulting film was either hydrated with 1× PBS or solvated with hexadecane. In the aqueous buffer, the liposome solution was subjected to four freeze–thaw cycles, followed by extrusion through Whatman track-etched polycarbonate 100 nm membranes to create monodisperse populations of unilamellar liposomes. Aqueous liposome solutions were stored at 4 °C. If the lipid film was solvated with hexadecane instead, the hexadecane/lipid mixture was simply vortexed until fully dissolved, yielding inverse lipid micelles in oil. These samples were stored at room temperature and used within two weeks of preparation. All samples were vortexed again prior to use.

Dynamic Light Scattering and ζ-Potential. The hydrodynamic diameters of the nanoparticle and liposome solutions were measured using a Zetasizer Nano ZS dynamic light scattering (DLS) machine (ZEN3500, Malvern). Briefly, a sample was loaded into an appropriate cuvette and illuminated with a laser. The light backscattered at ∼175° was detected; the change in scattered light intensity over time correlated with the hydrodynamic diameters of the molecules. DLS measurements verified that aqueous liposome solutions had a narrow polydispersity index (PDI < 0.2) centered around 100 nm, while all nanoparticle solutions had a slightly higher polydispersity index (PDI < 0.35) with an average hydrodynamic diameter <10 nm. Both lipid and AuNP solutions showed little to no aggregation for at least one month after preparation. To measure the ζ-potential, aqueous samples were loaded into a folded capillary cell and placed in the Zetasizer Nano ZS system. Electrodes at either end of the capillary applied an electric potential across the aqueous solution, and the machine detected scattered light from the moving particles related to the electrophoretic mobility. The AuNPs in 1× PBS had a ζ-potential of *ca.* −41 mV, which is in agreement with prior studies.[11] DOPC and DPhPC liposomes had a ζ-potential of ∼0 mV, as expected.[52,53]

Pendant Drop Tensiometry. Pendant drop tensiometry was performed on a Dataphysics OCA 15EC device. To measure interfacial tensions, aqueous solutions were suspended vertically in a 250 μL syringe into a glass cuvette containing either neat hexadecane or a hexadecane/lipid solution. The syringe needle for these experiments was 0.72 mm in diameter and was coated in Teflon to avoid the aqueous solution clinging to the exterior surface. Single pendant droplets were dispensed at a designated dosing rate (μL/s) to a final volume, and a camera captured the changes in the droplet profile as the droplets remained suspended from the syringe. Droplets within compared test conditions were the same volume to ensure a consistent surface area and were dispensed slowly to avoid significant convection. Interfacial tension was calculated using a Laplace–Young fitting in Dataphysics SCA20 software. Experiments were performed at room temperature, where these lipids exist in a fluid thermotropic phase.[31]

To quantify differences in the rates of interfacial tension (IFT) reduction, the short-time approximation of the Ward–Tordai equation[32] was used to model the diffusion-controlled adsorption of individual surfactants to the liquid–liquid interface. The Henry isotherm was incorporated to relate the surface density to the measurable quantity of surface tension, yielding the equation[32]

$$\gamma(t)_{t\to 0} = \gamma_0 - D_{\text{eff}}\sqrt{t} \tag{1}$$

where

$$D_{\text{eff}} = 2nRTc_0\sqrt{\frac{D}{\pi}}$$

γ_0 is the surface tension at a neat interface, $\gamma(t)_{t\to 0}$ is the change in the surface tension shortly after the interface is formed, n = 1 or 2 for nonionic or ionic surfactants, respectively, R is the gas constant, T is the temperature, c_0 is the bulk concentration of the surfactant species, and D is the diffusion coefficient. Plotting the measured $\gamma(t)$ vs. $\sqrt{t}$ allowed for the identification of diffusion-limited adsorption in surfactant systems and the quantification of D_{eff}, the effective rate of lipid adsorption, via a linear fit to the data at early points in time (Figure S3). Student's *t*-tests on the collected data were performed in Matlab. Normal distributions of sample populations were qualitatively verified using $Q-Q$ plots.

Vibrational Sum Frequency Generation (SFG). SFG experiments were performed using an instrument detailed elsewhere.[54,55] Briefly, a broad-band mid-infrared (IR) light centered near 2900 cm^{-1} was colinearly combined with a narrow-band near-infrared light (NIR ∼1 nm, full width at half max at ∼800 nm) and focused on the liquid sample at a 60° angle with respect to the surface normal. After passing through the oil phase, the incident angles at the oil–aqueous interface were ∼37°.[17,56] Polarizations for both IR and NIR beams were varied with half-waveplates after being polarization purified using the appropriate polarizers. The radiated SFG was polarization purified and spectrally resolved in a spectrograph equipped with a CCD camera, which was used for detection. The liquid–liquid interface was prepared by depositing 10 μL of a hexadecane/lipid solution at 1 mM concentrations onto 7 mL of the aqueous phase containing 0.1 mg/mL AuNPs from which the SFG was immediately measured. The thickness of the oil layer was estimated to be <10 μm based on the size of the supporting Teflon dish and the volume added. The time resolution was set by the CCD camera exposure time of 90 s/frame. Letters describing the polarization combinations (*e.g.*, SSP) denote the polarization state of the SFG, NIR, and IR fields, respectively. Background-subtracted SFG spectra were scaled by a reference spectrum from a Au film taken under the same experimental conditions to correct for the IR spectral shape.

To extract molecular scale parameters captured by the SFG spectra, data were fit to

$$I_{\text{SFG}} \propto \left| \chi_{\text{NR}}^{(2)} e^{i\phi} + \sum_q \frac{A_q}{\omega_{\text{IR}} - \omega_q + i\Gamma_q} \right|^2 \tag{2}$$

where I_{SFG} is the measured SFG intensity, $\chi_{\text{NR}}^{(2)}$ is the nonresonant background with contributions from ordered water[57] via the third-order susceptibility, and ϕ is the phase angle. The parameters A_q, ω_q, and Γ_q are mode-specific amplitudes, resonant frequencies, and peak widths, respectively. A summary of the fitting parameters is provided in the Supporting Information. Orientational analyses followed the procedure detailed by Allen and co-workers,[43] whereas thePAF was defined according to the work of Petersen and co-workers.[58] Indices of refraction were taken to be 1.0, 1.434, 1.333, and 1.18 for air, hexadecane, water, and the interfacial monolayer, respectively.[38]

ASSOCIATED CONTENT

Supporting Information

The Supporting Information is available free of charge at https://pubs.acs.org/doi/10.1021/acsnano.1c02663.

Additional pendant drop tensiometer measurements and linear regressions of interfacial tension data, images of saturated monolayer compression, tables summarizing SFG fitting parameters, SFG spectra at the air–aqueous interface, and time-resolved SFG data discussed in the text (PDF)

AUTHOR INFORMATION

Corresponding Authors

Benjamin Doughty − *Chemical Sciences Division, Oak Ridge National Laboratory, Oak Ridge, Tennessee 37831, United*

https://doi.org/10.1021/acsnano.1c02663
ACS Nano 2021, 15, 14285−14294

States; orcid.org/0000-0001-6429-9329; Email: doughtybl@ornl.gov

Stephen A. Sarles − *Mechanical Aerospace and Biomedical Engineering, University of Tennessee, Knoxville, Tennessee 37996, United States;* orcid.org/0000-0002-6694-6451; Email: ssarles@utk.edu

Authors

Colin M. Basham − *Mechanical Aerospace and Biomedical Engineering, University of Tennessee, Knoxville, Tennessee 37996, United States;* orcid.org/0000-0002-4364-221X

Uvinduni I. Premadasa − *Chemical Sciences Division, Oak Ridge National Laboratory, Oak Ridge, Tennessee 37831, United States;* orcid.org/0000-0003-0289-2965

Ying-Zhong Ma − *Chemical Sciences Division, Oak Ridge National Laboratory, Oak Ridge, Tennessee 37831, United States;* orcid.org/0000-0002-8154-1006

Francesco Stellacci − *Institute of Materials, École Polytechnique Fédérale de Lausanne (EPFL), CH-1015 Lausanne, Switzerland;* orcid.org/0000-0003-4635-6080

Complete contact information is available at: https://pubs.acs.org/10.1021/acsnano.1c02663

Author Contributions

[▽]C.M.B. and U.I.P. contributed equally to this work. C.M.B. and S.A.S. designed and executed interfacial tension measurements and related modeling. U.I.P., Y.-Z.M., and B.D. designed and executed SFG measurements and related analyses. F.S. provided nanoparticles for the study. All authors contributed to the manuscript preparation and have given approval to the final version of the manuscript.

Notes

The authors declare no competing financial interest.

ACKNOWLEDGMENTS

U.I.P., B.D., and Y.-Z.M. were supported by the U.S. Department of Energy, Office of Science, Basic Energy Sciences, Chemical Sciences, Geosciences, and Biosciences Division. C.M.B. and S.A.S. acknowledge financial support from the National Science Foundation through CAREER Grant CBET-1752197. F.S. acknowledges financial support from the Swiss National Science Foundation, Division II grant.

REFERENCES

(1) Santini, E.; Guzmán, E.; Ferrari, M.; Liggieri, L. Emulsions Stabilized by the Interaction of Silica Nanoparticles and Palmitic Acid at the Water−Hexane Interface. *Colloids Surf., A* **2014**, *460*, 333−341.

(2) Cui, M.; Emrick, T.; Russell, T. P. Stabilizing Liquid Drops in Nonequilibrium Shapes by the Interfacial Jamming of Nanoparticles. *Science* **2013**, *342*, 460−463.

(3) Davis, M. E.; Chen, Z. G.; Shin, D. M. Nanoparticle Therapeutics: An Emerging Treatment Modality for Cancer. *Nat. Rev. Drug Discovery* **2008**, *7*, 771−782.

(4) Moghimi, S. M.; Hunter, A. C.; Murray, J. C. Nanomedicine: Current Status and Future Prospects. *FASEB J.* **2005**, *19*, 311−330.

(5) Van Lehn, R. C.; Atukorale, P. U.; Carney, R. P.; Yang, Y.-S.; Stellacci, F.; Irvine, D. J.; Alexander-Katz, A. Effect of Particle Diameter and Surface Composition on the Spontaneous Fusion of Monolayer-Protected Gold Nanoparticles with Lipid Bilayers. *Nano Lett.* **2013**, *13*, 4060−4067.

(6) Truong, N. P.; Whittaker, M. R.; Mak, C. W.; Davis, T. P. The Importance of Nanoparticle Shape in Cancer Drug Delivery. *Expert Opin. Drug Delivery* **2015**, *12*, 129−142.

(7) Zhao, L.; Seth, A.; Wibowo, N.; Zhao, C.-X.; Mitter, N.; Yu, C.; Middelberg, A. P. Nanoparticle Vaccines. *Vaccine* **2014**, *32*, 327−337.

(8) Sun, P.; Nowack, L. M.; Bu, W.; Bera, M. K.; Griesemer, S.; Reik, M.; Portner, J.; Rice, S. A.; Schlossman, M. L.; Lin, B. Free Thiols Regulate the Interactions and Self-Assembly of Thiol-Passivated Metal Nanoparticles. *Nano Lett.* **2021**, *21*, 1613.

(9) Clark, S. B.; Buchanan, M.; Wilmarth, B. *Basic Research Needs for Environmental Management*; PNNL-25166; Pacific Northwest National Lab: Richland, WA, 2016.

(10) Pallares, R. M.; Abergel, R. J. Transforming Lanthanide and Actinide Chemistry with Nanoparticles. *Nanoscale* **2020**, *12*, 1339−1348.

(11) Verma, A.; Uzun, O.; Hu, Y.; Hu, Y.; Han, H.-S.; Watson, N.; Chen, S.; Irvine, D. J.; Stellacci, F. Surface-Structure-Regulated Cell-Membrane Penetration by Monolayer-Protected Nanoparticles. *Nat. Mater.* **2008**, *7*, 588.

(12) Guo, Y.; Terazzi, E.; Seemann, R.; Fleury, J. B.; Baulin, V. A. Direct Proof of Spontaneous Translocation of Lipid-Covered Hydrophobic Nanoparticles through a Phospholipid Bilayer. *Science advances* **2016**, *2*, No. e1600261.

(13) Van Lehn, R. C.; Ricci, M.; Silva, P. H.; Andreozzi, P.; Reguera, J.; Voïtchovsky, K.; Stellacci, F.; Alexander-Katz, A. Lipid Tail Protrusions Mediate the Insertion of Nanoparticles into Model Cell Membranes. *Nat. Commun.* **2014**, *5*, 4482.

(14) Van Lehn, R. C.; Alexander-Katz, A. Energy Landscape for the Insertion of Amphiphilic Nanoparticles into Lipid Membranes: A Computational Study. *PLoS One* **2019**, *14*, No. e0209492.

(15) Carney, R. P.; Astier, Y.; Carney, T. M.; Voïtchovsky, K.; Jacob Silva, P. H.; Stellacci, F. Electrical Method to Quantify Nanoparticle Interaction with Lipid Bilayers. *ACS Nano* **2013**, *7*, 932−942.

(16) Carney, R. P.; Carney, T. M.; Mueller, M.; Stellacci, F. Dynamic Cellular Uptake of Mixed-Monolayer Protected Nanoparticles. *Biointerphases* **2012**, *7*, 17.

(17) Chowdhury, A. U.; Lin, L.; Doughty, B. Hydrogen-Bond-Driven Chemical Separations: Elucidating the Interfacial Steps of Self-Assembly in Solvent Extraction. *ACS Appl. Mater. Interfaces* **2020**, *12*, 32119−32130.

(18) Watson, B. R.; Ma, Y.-Z.; Cahill, J. F.; Doughty, B.; Calhoun, T. R. Probing Ligand Removal and Ordering at Quantum Dot Surfaces Using Vibrational Sum Frequency Generation Spectroscopy. *J. Colloid Interface Sci.* **2019**, *537*, 389−395.

(19) Schabes, B. K.; Altman, R. M.; Richmond, G. L. Come Together: Molecular Details into the Synergistic Effects of Polymer−Surfactant Adsorption at the Oil/Water Interface. *J. Phys. Chem. B* **2018**, *122*, 8582−8590.

(20) Robertson, E. J.; Richmond, G. L. Molecular Insights in the Structure and Layered Assembly of Polyelectrolytes at the Oil/Water Interface. *J. Phys. Chem. C* **2014**, *118*, 28331−28343.

(21) Chen, Y.; Jena, K. C.; Roke, S. From Hydrophobic to Hydrophilic: The Structure and Density of the Hexadecane Droplet/Alkanol/Water Interface. *J. Phys. Chem. C* **2015**, *119*, 17725−17734.

(22) Olenick, L. L.; Troiano, J. M.; Smolentsev, N.; Ohno, P. E.; Roke, S.; Geiger, F. M. Polycation Interactions with Zwitterionic Phospholipid Monolayers on Oil Nanodroplet Suspensions in Water (D2O) Probed by Sum Frequency Scattering. *J. Phys. Chem. B* **2018**, *122*, 5049−5056.

(23) Gruen, D. W.; Wolfe, J. Lateral Tensions and Pressures in Membranes and Lipid Monolayers. *Biochim. Biophys. Acta, Biomembr.* **1982**, *688*, 572−580.

(24) Taylor, G. J.; Venkatesan, G. A.; Collier, C. P.; Sarles, S. A. Direct *in Situ* Measurement of Specific Capacitance, Monolayer Tension, and Bilayer Tension in a Droplet Interface Bilayer. *Soft Matter* **2015**, *11*, 7592−7605.

(25) Maestro, A.; Santini, E.; Zabiegaj, D.; Llamas, S.; Ravera, F.; Liggieri, L.; Ortega, F.; Rubio, R. G.; Guzman, E. Particle and Particle-Surfactant Mixtures at Fluid Interfaces: Assembly, Morphology, and Rheological Description. *Adv. Condens. Matter Phys.* **2015**, *2015*, 1.

(26) Venkatesan, G. A.; Taylor, G. J.; Basham, C. M.; Brady, N. G.; Collier, C. P.; Sarles, S. A. Evaporation-Induced Monolayer

Compression Improves Droplet Interface Bilayer Formation Using Unsaturated Lipids. *Biomicrofluidics* **2018**, *12*, 024101.
(27) Staton, J. A.; Stearns, S. W.; Dungan, S. R. Mechanism of Time-Dependent Adsorption for Phosphatidylcholine onto a Clean Air−Water Interface from a Dispersion of Vesicles: Effect of Temperature and Acyl Chain Length. *Langmuir* **2019**, *35*, 16850−16861.
(28) Santini, E.; Guzmán, E.; Ravera, F.; Ferrari, M.; Liggieri, L. Properties and Structure of Interfacial Layers Formed by Hydrophilic Silica Dispersions and Palmitic Acid. *Phys. Chem. Chem. Phys.* **2012**, *14*, 607−615.
(29) Atukorale, P. U.; Guven, Z. P.; Bekdemir, A.; Carney, R. P.; Van Lehn, R. C.; Yun, D. S.; Jacob Silva, P. H.; Demurtas, D.; Yang, Y.-S.; Alexander-Katz, A.; et al. Structure−Property Relationships of Amphiphilic Nanoparticles That Penetrate or Fuse Lipid Membranes. *Bioconjugate Chem.* **2018**, *29*, 1131−1140.
(30) Tahir, M. A.; Guven, Z. P.; Arriaga, L. R.; Tinao, B.; Yang, Y.-S. S.; Bekdemir, A.; Martin, J. T.; Bhanji, A. N.; Irvine, D.; Stellacci, F.; et al. Calcium-Triggered Fusion of Lipid Membranes Is Enabled by Amphiphilic Nanoparticles. *Proc. Natl. Acad. Sci. U. S. A.* **2020**, *117*, 18470−18476.
(31) Venkatesan, G. A.; Lee, J.; Farimani, A. B.; Heiranian, M.; Collier, C. P.; Aluru, N. R.; Sarles, S. A. Adsorption Kinetics Dictate Monolayer Self-Assembly for Both Lipid-In and Lipid-Out Approaches to Droplet Interface Bilayer Formation. *Langmuir* **2015**, *31*, 12883−12893.
(32) Eastoe, J.; Dalton, J. Dynamic Surface Tension and Adsorption Mechanisms of Surfactants at the Air−Water Interface. *Adv. Colloid Interface Sci.* **2000**, *85*, 103−144.
(33) Ariel, G.; Diamant, H.; Andelman, D. Kinetics of Surfactant Adsorption at Fluid-Fluid Interfaces: Surfactant Mixtures. *Langmuir* **1999**, *15*, 3574−3581.
(34) Guzmán, E.; Santini, E.; Benedetti, A.; Ravera, F.; Ferrari, M.; Liggieri, L. Surfactant Induced Complex Formation and Their Effects on the Interfacial Properties of Seawater. *Colloids Surf., B* **2014**, *123*, 701−709.
(35) Shi, S.; Russell, T. P. Nanoparticle Assembly at Liquid−Liquid Interfaces: From the Nanoscale to Mesoscale. *Adv. Mater.* **2018**, *30*, 1800714.
(36) Whitby, C. P.; Fornasiero, D.; Ralston, J.; Liggieri, L.; Ravera, F. Properties of Fatty Amine−Silica Nanoparticle Interfacial Layers at the Hexane−Water Interface. *J. Phys. Chem. C* **2012**, *116*, 3050−3058.
(37) Chai, Y.; Lukito, A.; Jiang, Y.; Ashby, P. D.; Russell, T. P. Fine-Tuning Nanoparticle Packing at Water−Oil Interfaces Using Ionic Strength. *Nano Lett.* **2017**, *17*, 6453−6457.
(38) Wang, H.-F.; Gan, W.; Lu, R.; Rao, Y.; Wu, B.-H. Quantitative Spectral and Orientational Analysis in Surface Sum Frequency Generation Vibrational Spectroscopy (SFG-VS). *Int. Rev. Phys. Chem.* **2005**, *24*, 191−256.
(39) Premadasa, U. I.; Adhikari, N. M.; Cimatu, K. L. A. Molecular Insights into the Role of Electronic Substituents on the Chemical Environment of the -Ch3 and >C=O Groups of Neat Liquid Monomers Using Sum Frequency Generation Spectroscopy. *J. Phys. Chem. C* **2019**, *123*, 28201−28209.
(40) Olenick, L. L.; Troiano, J. M.; Vartanian, A.; Melby, E. S.; Mensch, A. C.; Zhang, L.; Hong, J.; Mesele, O.; Qiu, T.; Bozich, J.; Lohse, S.; Zhang, X.; Kuech, T. R.; Millevolte, A.; Gunsolus, I.; Mcgeachy, A. C.; Doğangün, M.; Li, T.; Hu, D.; Walter, S. R.; et al. Lipid Corona Formation from Nanoparticle Interactions with Bilayers. *Chem.* **2018**, *4*, 2709−2723.
(41) Weeraman, C.; Yatawara, A. K.; Bordenyuk, A. N.; Benderskii, A. V. Effect of Nanoscale Geometry on Molecular Conformation: Vibrational Sum-Frequency Generation of Alkanethiols on Gold Nanoparticles. *J. Am. Chem. Soc.* **2006**, *128*, 14244−14245.
(42) Kawai, T.; Neivandt, D. J.; Davies, P. B. Sum Frequency Generation on Surfactant-Coated Gold Nanoparticles. *J. Am. Chem. Soc.* **2000**, *122*, 12031−12032.
(43) Adams, E. M.; Verreault, D.; Jayarathne, T.; Cochran, R. E.; Stone, E. A.; Allen, H. C. Surface Organization of a Dppc Monolayer on Concentrated $SrCl_2$ and $ZnCl_2$ Solutions. *Phys. Chem. Chem. Phys.* **2016**, *18*, 32345−32357.
(44) Walker, R. A.; Conboy, J. C.; Richmond, G. L. Molecular Structure and Ordering of Phospholipids at a Liquid-Liquid Interface. *Langmuir* **1997**, *13*, 3070−3073.
(45) Walker, R.; Gragson, D.; Richmond, G. Induced Changes in Solvent Structure by Phospholipid Monolayer Formation at a Liquid−Liquid Interface. *Colloids Surf., A* **1999**, *154*, 175−185.
(46) Frederick, M. T.; Achtyl, J. L.; Knowles, K. E.; Weiss, E. A.; Geiger, F. M. Surface-Amplified Ligand Disorder in CdSe Quantum Dots Determined by Electron and Coherent Vibrational Spectroscopies. *J. Am. Chem. Soc.* **2011**, *133*, 7476−7481.
(47) Ravera, F.; Santini, E.; Loglio, G.; Ferrari, M.; Liggieri, L. Effect of Nanoparticles on the Interfacial Properties of Liquid/Liquid and Liquid/Air Surface Layers. *J. Phys. Chem. B* **2006**, *110*, 19543−19551.
(48) Santini, E.; Krägel, J.; Ravera, F.; Liggieri, L.; Miller, R. Study of the Monolayer Structure and Wettability Properties of Silica Nanoparticles and CTAB Using the Langmuir Trough Technique. *Colloids Surf., A* **2011**, *382*, 186−191.
(49) Canepa, E.; Salassi, S.; De Marco, A. L.; Lambruschini, C.; Odino, D.; Bochicchio, D.; Canepa, F.; Canale, C.; Dante, S.; Brescia, R.; et al. Amphiphilic Gold Nanoparticles Perturb Phase Separation in Multidomain Lipid Membranes. *Nanoscale* **2020**, *12*, 19746−19759.
(50) Lane, J. M. D.; Grest, G. S. Spontaneous Asymmetry of Coated Spherical Nanoparticles in Solution and at Liquid-Vapor Interfaces. *Phys. Rev. Lett.* **2010**, *104*, 235501.
(51) Böckmann, R. A.; Hac, A.; Heimburg, T.; Grubmüller, H. Effect of Sodium Chloride on a Lipid Bilayer. *Biophys. J.* **2003**, *85*, 1647−1655.
(52) Dos Santos Cabrera, M. P.; Arcisio-Miranda, M.; Gorjao, R.; Leite, N. B.; De Souza, B. M.; Curi, R.; Procopio, J.; Ruggiero Neto, J.; Palma, M. S. Influence of the Bilayer Composition on the Binding and Membrane Disrupting Effect of Polybia-MP1, an Antimicrobial Mastoparan Peptide with Leukemic T-Lymphocyte Cell Selectivity. *Biochemistry* **2012**, *51*, 4898−4908.
(53) Pohl, E. E.; Krylov, A. V.; Block, M.; Pohl, P. Changes of the Membrane Potential Profile Induced by Verapamil and Propranolol. *Biochim. Biophys. Acta, Biomembr.* **1998**, *1373*, 170−178.
(54) Chowdhury, A. U.; Liu, F.; Watson, B. R.; Ashkar, R.; Katsaras, J.; Collier, C. P.; Lutterman, D. A.; Ma, Y.-Z.; Calhoun, T. R.; Doughty, B. Flexible Approach to Vibrational Sum-Frequency Generation Using Shaped Near-Infrared Light. *Opt. Lett.* **2018**, *43*, 2038−2041.
(55) Chowdhury, A. U.; Watson, B. R.; Ma, Y.-Z.; Sacci, R. L.; Lutterman, D. A.; Calhoun, T. R.; Doughty, B. A New Approach to Vibrational Sum Frequency Generation Spectroscopy Using near Infrared Pulse Shaping. *Rev. Sci. Instrum.* **2019**, *90*, 033106.
(56) Chowdhury, A. U.; Taylor, G. J.; Bocharova, V.; Sacci, R. L.; Luo, Y.; Mcclintic, W. T.; Ma, Y.-Z.; Sarles, S. A.; Hong, K.; Collier, C. P.; et al. Insight into the Mechanisms Driving the Self-Assembly of Functional Interfaces: Moving from Lipids to Charged Amphiphilic Oligomers. *J. Am. Chem. Soc.* **2020**, *142*, 290−299.
(57) Ohno, P. E.; Wang, H.-F.; Geiger, F. M. Second-Order Spectral Lineshapes from Charged Interfaces. *Nat. Commun.* **2017**, *8*, 1032.
(58) Barrett, A.; Petersen, P. B. Order of Dry and Wet Mixed-Length Self-Assembled Monolayers. *J. Phys. Chem. C* **2015**, *119*, 23943−23950.

https://doi.org/10.1021/acsnano.1c02663
ACS Nano 2021, 15, 14285−14294